Conformational Dynamics of Propane, Di-*tert*-butylmethane, and Bis(9-triptycyl)methane. An Analysis of the Symmetry of Two 3-fold Rotors on a Rigid Frame in Terms of Nonrigid Molecular Structure and Energy Hypersurfaces

Hans-Beat Bürgi,*[1a] W. Douglas Hounshell,[1b] Robert B. Nachbar, Jr.,[1c] and Kurt Mislow*[1c]

Contribution from the Laboratorium für chemische und mineralogische Kristallographie der Universität, 3012-Bern, Switzerland, Molecular Design, Ltd., Hayward, California 94541, and the Department of Chemistry, Princeton University, Princeton, New Jersey 08544.
Received May 10, 1982

Abstract: Analysis of molecular symmetry is combined with empirical force field calculations to provide a basis for describing internal motions in three types of molecules comprised of two threefold rotors on a C_{2v} frame: propane (**1**), di-*tert*-butylmethane (**2**), and bis(9-triptycyl)methane (**3**). The molecular symmetry group of these systems is $G_{36} = (C_3 \times C_3) \wr V$ (of order 36). A representation of this group in terms of the rotor conformational angles shows a close relationship to a crystallographic plane group and furnishes a pictorial map of changes in geometry during conformational interconversions. Potential energy surfaces relevant to such changes were calculated by the empirical force field (EFF) method for all three systems by using full matrix Newton–Raphson optimization together with the force field from the MM2 program. Salient features of the internal motions in **1–3** are described. The calculations reveal that **3** undergoes correlated disrotation (dynamic gearing) of the 9-triptycyl (Tp) groups as a virtually unhindered process, with a barrier of 0.19 kcal mol^{-1}, whereas gear slippage (net conrotation of the Tp groups) requires at least 30.1 kcal mol^{-1}. The mechanism of gear slippage is found by calculation to involve a transition state in which two benzene rings within one Tp moiety are squeezed together and tucked into the notch between two rings in the other Tp group. The stereochemical consequences of these interconversion mechanisms on labeled variants of all three compounds are analyzed by using group theory. The results are given in terms of the type and number of residual stereoisomers expected for each type of labeled molecule under the operation of those interconversion processes that are found to be energetically feasible according to the EFF calculations. The minimal labeling of **3** is deduced that allows a distinction between gearing with and without gear slippage.

The coupled disrotation of chemical rotors evokes an image of meshed cogwheels in motion. Two coupling mechanisms are conceivable for such dynamic gearing. In the first of these, coupling originates in nonbonded interactions betwen tightly intermeshed groups, as might be expected for sterically crowded molecules. It is here that the analogy between chemical and mechanical gears is most aptly applied. Recently, aspects of this mechanism were analyzed critically.[2] In the other, concerted torsions result from orbital symmetry control.[3] The present report investigates—from a theoretical perspective—internal motions governed by steric factors.[4]

In our view, any system chosen for such a study has to meet at least three requirements: first, the need for simplicity, and hence for a system limited to two rotors of the same periodicity; second, the need to remain faithful to the central analogy of cogwheels, and hence for a system in which the two rotor axes are not coaxial;[5] and, third, the need to maximize the opportunity for strong coupling (intermeshing), and hence for a sterically crowded molecular system.[6]

In a literature that abounds in studies of coupled rotations and gear effects,[7,8] there is no dearth of candidates that meet the above requirements.[9] In the selection of systems for the present study,

(1) (a) Universität Bern. (b) Molecular Design, Ltd. (c) Princeton University.

(2) Hounshell, W. D.; Iroff, L. D.; Iverson, D. J.; Wroczynski, R. J.; Mislow, K. *Isr. J. Chem.* **1980**, *20*, 65. See also: Hounshell, W. D.; Iroff, L. D.; Wroczynski, R. J.; Mislow, K. *J. Am. Chem. Soc.* **1978**, *100*, 5212. Iroff, L. D. *J. Comput. Chem.* **1980**, *1*, 76.

(3) An example is the disrotatory correlated rotation about the $Co_3(C-O)_9-C$ and $C-CH_2$ axes in $Co_3(CO)_9CCH_2^+$. See: Schilling, B. E. R.; Hoffmann, R. *J. Am. Chem. Soc.* **1978**, *100*, 6274; **1979**, *101*, 3456. Edidin, R. T.; Norton, J. R.; Mislow, K. *Organometallics* **1982**, *1*, 561.

(4) For a preliminary report, see: Hounshell, W. D.; Johnson, C. A.; Guenzi, A.; Cozzi, F.; Mislow, K. *Proc. Natl. Acad. Sci. U.S.A.* **1980**, *77*, 6961.

(5) Gear shafts may lie in the same plane (spur and bevel gears have parallel and intersecting axes, respectively) or in parallel planes with inclined axes. For a classification of the disposition of gear shafts, see: Watson, H. J. "Modern Gear Production"; Pergamon Press: Oxford, 1970.

(6) On the topic of sterically crowded molecules, see: Tidwell, T. T. *Tetrahedron* **1978**, *34*, 1855.

(7) Relevant citations to the literature are collected in ref 2.

(8) Torsional frequencies in molecules with geminal or vicinal methyl groups have been analyzed in terms of Fourier series that include terms corresponding to coupled rotation of methyl rotors. See, for example: (a) Lide, D. R., Jr.; Mann, D. E. *J. Chem. Phys.* **1958**, *28*, 572; *Ibid.* **1958**, *29*, 914. (b) Swalen, J. D.; Costain, C. C. *Ibid.* **1959**, *31*, 1562. (c) Rush, J. J. *Ibid.* **1967**, *47*, 3936. (d) Dreizler, H.; Sutter, D. *Z. Naturforsch. A* **1969**, *24A*, 2013. (e) Grant, D. M.; Pugmire, R. J.; Livingston, R. C.; Strong, K. A.; McMurray, H. L.; Brugger, R. M. *J. Chem. Phys.* **1970**, *52*, 4424. (f) Burnell, E. E.; Diehl, P. *Mol. Phys.* **1972**, *24*, 489. (g) Burnell, E. E.; Diehl, P. *Org. Magn. Reson.* **1973**, *5*, 137. (h) Livingston, R. C.; Grant, D. M.; Pugmire, R. J.; Strong, K. A.; Brugger, R. M. *J. Chem. Phys.* **1973**, *58*, 1438. (i) Durig, J. R.; Craven, S. M.; Mulligan, J. H.; Hawley, C. W.; Bragin, J. *Ibid.* **1973**, *58*, 1281. (j) Rojhantalab, H.; Nibler, J. W.; Wilkins, C. J. *Spectrochim. Acta, Part A* **1976**, *32A*, 519. (k) Durig, J. R.; Groner, P.; Griffin, M. G. *J. Chem. Phys.* **1977**, *66*, 3061. (l) Groner, P.; Durig, J. R. *Ibid.* **1977**, *66*, 1856. (m) Durig, J. R.; Griffin, M. G.; Groner, P. *J. Phys. Chem.* **1977**, *81*, 554. (n) Durig, J. R.; Compton, D. A. C. *J. Chem. Phys.* **1978**, *69*, 4713. (o) Durig, J. R.; Compton, D. A. C. *J. Phys. Chem.* **1979**, *83*, 265. (p) Durig, J. R.; Compton, D. A. C.; Jalilian, M.-R. *Ibid.* **1979**, *83*, 511. (q) Durig, J. R.; Compton, D. A. C. *Ibid.* **1979**, *83*, 2873. (r) Radom, L.; Pople, J. A. *J. Am. Chem. Soc.* **1970**, *92*, 4786. (s) Tang, J.; Pines, A. *J. Chem. Phys.* **1980**, *73*, 2512. (t) Hirota, E.; Matsumura, C.; Morino, Y. *Bull. Chem. Soc. Jpn.* **1967**, *40*, 1124. (u) Hoyland, J. R. *J. Chem. Phys.* **1968**, *49*, 1908. (v) Durig, J. R.; Compton, D. A. C.; Rizzolo, J. J.; Jalilian, M. R.; Zozulin, A. J.; Odom, J. D. *J. Mol. Struct.* **1981**, *77*, 195.

(9) As a notable example, we single out the study of Kwart and Alekman[10] of internal rotations in the dimesitylcarbinyl system, which led to the postulation of a "cogwheel effect". The correlated rotation of aryl rings in systems containing two such rings attached to a single atom (Ar_2Z) have been described and classified.[11] The permutational consequences of the one-ring flip are satisfied by an internal motion in which the two aryl rings rotate in synchrony, so that when one ring is in the C–Z–C plane, the other is perpendicular to it. In crowded systems, i.e., in systems containing phenyl rings with ortho substituents, this cogwheeling motion corresponds to the lowest energy pathway, with ground and transition states assuming helical and perpendicular conformations,[11] respectively.

(10) Kwart, H.; Alekman, S. *J. Am. Chem. Soc.* **1968**, *90*, 4482.

(11) Gust, D.; Mislow, K. *J. Am. Chem. Soc.* **1973**, *95*, 1535.

0002-7863/83/1505-1427$01.50/0

Table I. Class Structure of the MSG G_{36} Represented in Terms of Permutations and of Torsion Angles Describing Isometric Structures

group element no.	conjugacy class	permutations and permutation–inversions	transformations[a] ϕ	transformations[a] ϕ'	space group orientation
1	1	(1)	x	y	identity
2	2	(123)	$x + (2\pi/3)$	y	single translation
3		(132)	$x - (2\pi/3)$	y	
4		(456)	x	$y - (2\pi/3)$	
5		(465)	x	$y + (2\pi/3)$	
6	3	(123)(465)	$x + (2\pi/3)$	$y + (2\pi/3)$	symmetric translation
7		(132)(456)	$x - (2\pi/3)$	$y - (2\pi/3)$	
8	4	(123)(456)	$x + (2\pi/3)$	$y - (2\pi/3)$	antisymmetric translation
9		(132)(465)	$x - (2\pi/3)$	$y + (2\pi/3)$	
10	5	(14)(26)(35)(ab)	y	x	positive diagonal mirror reflection
11		(15)(24)(36)(ab)	$y + (2\pi/3)$	$x - (2\pi/3)$	
12		(16)(25)(34)(ab)	$y - (2\pi/3)$	$x + (2\pi/3)$	
13	6	(142635)(ab)	$y + (2\pi/3)$	x	positive diagonal glide reflection
14		(143526)(ab)	$y - (2\pi/3)$	x	
15		(152436)(ab)	$y - (2\pi/3)$	$x - (2\pi/3)$	
16		(153624)(ab)	y	$x - (2\pi/3)$	
17		(162534)(ab)	y	$x + (2\pi/3)$	
18		(163425)(ab)	$y + (2\pi/3)$	$x + (2\pi/3)$	
19	7	(12)(45)(ab)*	$-x + (2\pi/3)$	$-y - (2\pi/3)$	twofold rotation
20		(12)(46)(ab)*	$-x + (2\pi/3)$	$-y + (2\pi/3)$	
21		(12)(56)(ab)*	$-x + (2\pi/3)$	$-y$	
22		(13)(45)(ab)*	$-x - (2\pi/3)$	$-y - (2\pi/3)$	
23		(13)(46)(ab)*	$-x - (2\pi/3)$	$-y + (2\pi/3)$	
24		(13)(56)(ab)*	$-x - (2\pi/3)$	$-y$	
25		(23)(45)(ab)*	$-x$	$-y - (2\pi/3)$	
26		(23)(46)(ab)*	$-x$	$-y + (2\pi/3)$	
27		(23)(56)(ab)*	$-x$	$-y$	
28	8	(14)(25)(36)*	$-y$	$-x$	negative diagonal mirror reflection
29		(15)(26)(34)*	$-y - (2\pi/3)$	$-x - (2\pi/3)$	
30		(16)(24)(35)*	$-y + (2\pi/3)$	$-x + (2\pi/3)$	
31	9	(142536)*	$-y + (2\pi/3)$	$-x$	negative diagonal glide reflection
32		(143625)*	$-y - (2\pi/3)$	$-x$	
33		(152634)*	$-y$	$-x - (2\pi/3)$	
34		(153426)*	$-y + (2\pi/3)$	$-x - (2\pi/3)$	
35		(162435)*	$-y - (2\pi/3)$	$-x + (2\pi/3)$	
36		(163524)*	$-y$	$-x + (2\pi/3)$	

[a] In rad modulo 2π. See text.

we limited ourselves to a skeleton consisting of two threefold rotors attached to a rigid frame of local C_{2v} symmetry. This system is exemplified by propane (**1**), which, as the simplest hydrocarbon of this type, is included in our study for purposes of comparison even though the requirement of steric crowding is obviously not met. Obviously, this requirement *is* met in the derivative of **1** in which the six hydrogens in the methyl rotors are replaced by six methyl groups, i.e., di-*tert*-butylmethane (**2**). This compound, whose structure has been determined by gas-phase electron diffraction,[12] has a central C–CH_2–C angle of 125–128°,[13] indicative of considerable internal congestion. As the third and most crowded representative, we selected bis(9-triptycyl)methane (**3**), a molecule whose inclusion in our study owed its inspiration, in a general way, to the pioneering studies by Ōki and co-workers on hindered rotation in 9-substituted triptycenes,[14] and, more specifically, to the report in 1979 by Yamamoto and Ōki[15] suggesting a cogwheel effect in 9-benzyltriptycene derivatives.[16]

The problem of describing the structure and energy of these conformationally flexible molecules will be dealt with in two consecutive steps: first, group theory is used to analyze the symmetry of the system, and, second, energy changes that accompany conformational changes are calculated by the empirical force field (EFF) method. Following a description of this approach and of parts of the Born–Oppenheimer potential energy (PE) surfaces calculated for **1**–**3**, we go on to consider the rearrangement modes of these compounds. An analysis of isomerism in suitably labeled derivatives provides the theoretical background for an experimental test of gearing.

Methods

Permutation Group Approach. The treatment of chemical isomerizations and homomerizations (or automerizations) of nonrigid molecules in terms of ligand permutations has proven to be a convenient approach to dynamic stereochemistry.[17-19] For molecules such as **1**–**3**, in which

(12) Bartell, L. S.; Bradford, W. F. *J. Mol. Struct.* **1977**, *37*, 113.

(13) X-ray structures of related compounds yield values close to the lower limit of this range: (a) 126° (Bunn, C. W.; Holmes, D. R. *Discuss. Faraday Soc.* **1958**, *25*, 95). (b) 122.6° (Benedetti, E.; Pedone, C.; Allegra, G. *Macromolecules* **1970**, *3*, 16). (c) 123.8 and 124.1° (Adiwidjaja, G.; Voss, J. *Chem. Ber.* **1976**, *109*, 761). (d) 123.1 and 123.8° (McKinnon, B. J.; de Mayo, P.; Payne, N. C.; Ruge, B. *Nouv. J. Chem.* **1978**, *2*, 91). (e) 125.0° (Ermer, O.; Bödecker, C.-D. *Chem. Ber.* **1981**, *114*, 652).

(14) Ōki, M. *Angew. Chem., Int. Ed. Engl.* **1976**, *15*, 87 and referencess therein.

(15) Yamamoto, G.; Ōki, M. *Chem. Lett.* **1979**, 1251, 1255; *Bull. Chem. Soc. Jpn.* **1981**, *54*, 473, 481.

(16) Strictly speaking, the rotors in **2** are not directly comparable to those in **1** and **3**, for whereas the methyl groups in **1** and the triptycyl groups in **3** may be considered as rigid entities, the *tert*-butyl groups in **2** are not rigid.

(17) Ruch, E.; Hässelbarth, W.; Richter, B. *Theor. Chim. Acta* **1970**, *19*, 288. Hässelbarth, W.; Ruch, E. *Ibid.* **1973**, *29*, 259.

(18) Klemperer, W. G. *J. Chem. Phys.* **1972**, *56*, 5478; *J. Am. Chem. Soc.* **1972**, *94*, 6940; **1973**, *95*, 380. Brocas, J.; Willem, R. *Bull. Soc. Chim. Belg.* **1973**, *82*, 469.

(19) For work from this laboratory, see, for example: (a) Mislow, K. *Acc. Chem. Res.* **1976**, *9*, 26. (b) Hutchings, M. G.; Nourse, J. G.; Mislow, K. *Tetrahedron* **1974**, *30*, 1535. (c) Nourse, J. G.; Mislow, K. *J. Am. Chem. Soc.* **1975**, *97*, 4571. (d) Finocchiaro, P.; Hounshell, W. D.; Mislow, K. *Ibid.* **1976**, *98*, 4952.

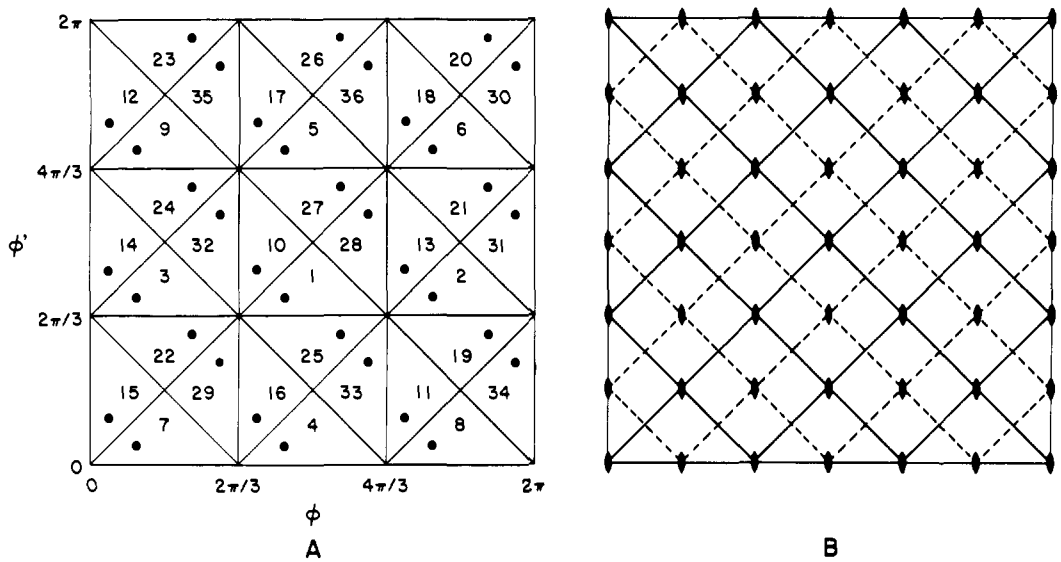

Figure 1. (A) The 36 equivalent triangles within the $2\pi \times 2\pi$ space spanned by (ϕ, ϕ'). The numbers correspond to the appropriate group element (Table I), with the identity triangle marked 1. The 36 dots represent equivalent general positions (x, y) that correspond to isometric structures. (B) Diagram of symmetry elements in space group $c2mm$ 3^2, a subgroup modulo 2π of the two-dimensional space group cmm, showing twofold rotation points (⧫), mirror reflection lines (—), and glide reflection lines (- - -).

the nonrigidity is due principally to internal torsional motions, the permutations of the ligands among the sites of the skeleton (A)[20] may be

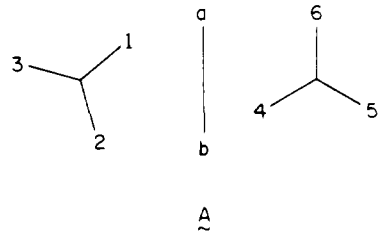

A

expressed by the Longuet-Higgins molecular symmetry group (MSG) of feasible rearrangements.[21] Specifically, this group includes (a) cyclic permutations (123) and (456), whose physical realizations will be in terms of internal rotation of one, the other, or both ligands; (b) pairwise interchange (14)(26)(35)(ab), corresponding to changing the conformational angle of one ligand to the value of the other ligand and vice versa; and (c) permutation–inversion (14)(25)(36)*, corresponding to rotation of one ligand to the negative conformational angle of the other and vice versa. Combinations of these operations (generators) leads to the relevant MSG of order 36, G_{36}.[22] This group may also be expressed[23] as the semidirect product $(C_3 \times C_3) \wedge V$, where the direct product $(C_3 \times C_3)$ is the torsional subgroup of order 9 that represents all possible combinations of cyclic permutations within the two threefold rotors and V is the frame subgroup of order four, which is isomorphic to C_{2v} and which expressed the symmetry of the C–CH_2–C frame.[24] The elements of the full group are arranged according to conjugacy classes in column 3 of Table I. Each corresponds to a torsional rearrangement of the molecule.

Space Group Approach. The permutation group approach does not usually necessitate a description of the detailed changes in geometry during conformational interconversions, i.e., of the reaction path. The space group approach, however, does provide such a description since it must be based on a suitable geometric representation of the problem.[25] Let us consider the case of propane, whose structure is completely specified by 27 ($3N - 6$, $N = 11$) linearly independent parameters; of these 10 may be chosen as bond lengths, 15 as bond angles. The remaining two, ϕ and ϕ', specify the conformations of the methyl rotors. The two-dimensional subspace defined by (ϕ, ϕ') provides a pictorial map of all conformations (stable and unstable) and a basis for describing interconversions among them. Analogous maps may be constructed for **2**, if we take the methyl groups as isotropic,[26] and for **3** with its rigid triptycyl groups.

The symmetry of such maps is isomorphic to G_{36}. To show this isomorphism, we need to determine all pairs of values (x, y) of the coordinates (ϕ, ϕ') corresponding to isometric structures.[27] Let us assume that the rotors have C_{3v} symmetry (deviations from this symmetry will be dealt with later). Then application of the permutation (123) effects the transformation $(x, y) \rightarrow (x + (2\pi/3) \pmod{2\pi}, y)$ and (456) effects $(x, y) \rightarrow (x, y - (2\pi/3) \pmod{2\pi})$, corresponding to the torsion of the individual rotors by $2\pi/3$; these permutations generate nine transformations which form a group isomorphic to the torsional subgroup $(C_3 \times C_3)$ of G_{36}. Furthermore, exchanging x and y leads to isometric structures because the two rotors are chemically identical, and changing signs of x and y also leads to isometric structures because the substituents 1, 2, 3 (and 4, 5, 6) are chemically identical and achiral. These last two exchanges are generators of a group of transformations of order 4, which is isomorphic to the frame subgroup V of G_{36}. The transformations of (x, y) described above thus form a group isomorphic to G_{36}, the elements of which are listed in column 4 of Table I.[28]

The isomorphism between G_{36} and the group of transformations attainable within the $2\pi \times 2\pi$ square spanned by (ϕ, ϕ') is thus established. The torsional subgroup of transformations maps a given $(2\pi/3) \times (2\pi/3)$ square onto one of nine such squares. Similarly, the frame subgroup maps a given rectangular isosceles triangle of hypothenuse 2π onto four such triangles. The $2\pi \times 2\pi$ square is thus partitioned into 36 equivalent rectangular isosceles triangles of hypothenuse $2\pi/3$ (asymmetric unit) by a combination of these mappings. Figure 1A shows a $2\pi \times 2\pi$ square thus partitioned, with each triangle labeled with a number corresponding

(20) Skeleton A is a schematic projection of the propane framework, with the labeled ligands (1–6 and a–b are methyl and methylene hydrogens, respectively) in their respective reference sites.

(21) Longuet-Higgins, H. C. *Mol. Phys.* **1963**, *6*, 445.

(22) This group is isomorphic to the MSG of ethane, whose character table has been given.[21]

(23) Woodman, C. M. *Mol. Phys.* **1970**, *19*, 753.

(24) The elements of V are e, (14)(26)(35)(ab), (23)(56)(ab)*, (14)(25)(36)*.

(25) (a) Murray-Rust, P.; Bürgi, H.-B.; Dunitz, J. D. *Acta Crystallogr., Sect. A* **1979**, *A35*, 703. (b) Dunitz, J. D. "X-ray Analysis and the Structure of Organic Molecules"; Cornell University Press: Ithaca, NY, 1979. (c) Bürgi, H.-B. *MATCH* **1980**, *9*, 13.

(26) Inclusion of individual methyl group rotations would bring the problem to an unmanageable level: the MSG is given by $((C_3)^3 \wedge C_3)^2 \wedge V$, a group of order 26 244. Similarly, for purposes of labeling and isomer enumeration (see below), we regard each methyl group as a single unit; that is, we distinguish among different methyl groups but not among the hydrogens within each group.

(27) Two structures are isometric if they are properly or improperly congruent. Alternatively, nuclear configurations are isometric if their labeled graphs are the same, the labeling being by nuclear charge and mass for the vertices and by internuclear distances for the edges (Bauder, A.; Meyer, R.; Günthard, H. H. *Mol. Phys.* **1974**, *28*, 1305).

(28) The group of transformations may be expressed as a group of matrices acting on the vector $[x, y, 1]^T$. The generators of the group are

$$\begin{bmatrix} 1 & 0 & 2\pi/3 \\ 0 & 1 & 0 \\ 0 & 0 & 1 \end{bmatrix} \begin{bmatrix} 1 & 0 & 0 \\ 0 & 1 & 2\pi/3 \\ 0 & 0 & 1 \end{bmatrix} \begin{bmatrix} 0 & 1 & 0 \\ 1 & 0 & 0 \\ 0 & 0 & 1 \end{bmatrix} \begin{bmatrix} -1 & 0 & 0 \\ 0 & -1 & 0 \\ 0 & 0 & 1 \end{bmatrix}$$

Table II. Comparison of Molecular Symmetry with Space Group Symmetry

conformation		symmetry		number of isometric structures or equivalent positions (N)
ϕ	ϕ'	$c2mm$ 3^2 (p)[a]	molecular[b]	
0	0	mm (a)	$C_{2v}(1/1)$	9
$2\pi/6$	$2\pi/6$	mm (b)	$C_{2v}(2/2)$	9
0	$2\pi/6$	2 (c)	$C_s(1/2)$	18
x	x	m (d)	C_2	18
x	$-x$	m (e)	C_s	18
x	y	1 (f)	C_1	36

[a] Site symmetry of the function $E(\phi, \phi')$ and, in parentheses, Wyckoff notation as listed in ref 30. [b] In this notation, the parenthesized descriptors following the point group symbols indicate "gear-clashed" (1/1 or 2/2) or "geared" (2/1 or 1/2) conformations.

to an element in the group of transformations (cf. Table I, columns 1 and 4).

To illustrate the relationships between pairs of triangles in Figure 1A and the corresponding transformations, let us consider a general point (x, y) within the triangle marked 1 (T_1, the identity triangle). The transformation corresponding to group element 6 $(x + (2\pi/3), y + (2\pi/3))$ sends this point into the equivalent position within T_6; similarly, the transformations corresponding to group elements 18, 20, and 30 send the point in T_1 into equivalent positions within T_{18}, T_{20}, and T_{30}. We may view the $2\pi \times 2\pi$ square in Figure 1A as a finite subspace of an infinite, two-dimensional lattice, and the associated group of transformations of order 36 as a subgroup modulo 2π of an infinite group,[29] which has long been known in crystallography as the two-dimensional space group (or plane group) cmm ($\equiv c2mm$).[30] It is obvious merely by inspection of the pattern of points in Figure 1A (developed as described above) that these points are related by the combination of reflection, rotation, and translation operations of cmm that are shown in Figure 1B and listed in the rightmost column of Table I. The subgroup modulo 2π will be designated by $c2mm$ 3^2(p), where $2mm$ represents the motif symmetry within a $(2\pi/3) \times (2\pi/3)$ unit cell,[31] 3^2 represents the threefold translational periodicity in each dimension (corresponding to the division of the $2\pi \times 2\pi$ square into nine $(2\pi/3) \times (2\pi/3)$ squares), c refers to the centered lattice used in the standard representation of this group,[32] and (p) indicates that we specify the translational periodicity with respect to the nonstandard primitive lattice on the basis of the coordinates (ϕ, ϕ'). According to this notation, subgroups V and $(C_3 \times C_3)$ are isomorphic to subgroups $c2mm$ 1^2 (p) and $p111$ 3^2, respectively. Conformations of 1, **2**, or **3** with C_1 symmetry are mapped onto one of the 36 general positions (x, y) within $c2mm$ 3^2 (p). Conformations with higher symmetry are mapped onto special positions (Table II). Now let us consider a molecular property, e.g., the PE, as a function of (ϕ, ϕ'): the value of this function must be the same for (x, y) pairs describing isometric structures. The PE hypersurface of **1**–**3** will therefore have the same symmetry properties as the space spanned by (ϕ, ϕ'), i.e., $c2mm$ 3^2 (p), and a graphical representation of the hypersurface (e.g., a two-dimensional contour map) will show the symmetry of Figure 1B.

Potential Energy Functions. Strictly speaking, the PE surfaces of the molecules **1**–**3** depend in a complicated way on $3N - 6$ structural coordinates. However, all we need is that part of the PE surface which is relevant to the conformational interconversion processes. We may therefore choose to determine the conformational energy map $E'(\phi, \phi')$ for a model of rigid C_{3v} rotors on a rigid C_{2v} frame with all bond lengths d_i and bond angles α_j fixed at standard values (d_{i0}, α_{j0}). This corresponds to calculating a two-dimensional section through the full PE surface. Such a section $E'(\phi, \phi') = E(\phi, \phi', d_{i0}, \alpha_{j0})$ must be invariant under the operations of $c2mm$ 3^2 (p). This approach, although conceptually simple, represents an unnecessary simplification. An improved PE surface $E(\phi, \phi')$ may be obtained by allowing variations in the bond lengths and bond angles as a function of ϕ and ϕ', i.e., $E(\phi, \phi') = E(\phi, \phi', d_i(\phi, \phi'), \alpha_j(\phi, \phi'))$, where the planar section has been replaced by a rippled section defined by $(\phi, \phi', d_i(\phi, \phi'), \alpha_j(\phi, \phi'))$. Such a rippled section may be termed a reaction surface, in close analogy to a reaction coordinate that is very often represented as a linear coordinate, even though in actual fact it may be curved in the multidimensional space of bond lengths and angles.

An understanding of the function $E(\phi, \phi', d_i(\phi, \phi'), \alpha_j(\phi, \phi')$ necessitates an understanding of the transformation properties of the functions $d_i(\phi, \phi')$ and $\alpha_j(\phi, \phi')$ and their behavior for special values of ϕ, ϕ'. There are two types of such functions. First, there are those that are symmetric under a transformation of ϕ, ϕ' by an operation of $c2mm$ 3^2 (p), e.g., the central angle $\alpha_{CCC}(\phi', \phi) = \alpha_{CCC}(\phi, \phi')$. For these, an arbitrary value of the function is compatible with both general and special values of ϕ, ϕ', i.e., with trivial and nontrivial covering symmetries of the corresponding conformations. Second, there are those functions $d_i(\phi, \phi')$ or $\alpha_j(\phi, \phi')$ whose values are permuted with those of other functions on transforming ϕ, ϕ', e.g., the two central C–C bond lengths for which $d(\phi', \phi) = d'(\phi, \phi')$. The values of the permuting functions for general values of ϕ, ϕ' may be arbitrary, but for special values of ϕ, ϕ', some of them must be equal if the corresponding molecular symmetry is to be preserved; in the above example, $d(\phi, \phi') = d'(\phi, \phi')$ for $\phi = \phi'$. Indeed, for **1** and **2**, molecular symmetry was preserved for all special values of ϕ, ϕ'. In these examples it is in general sufficient to speak of a two-dimensional reaction surface $E(\phi, \phi')$ as defined in the preceding paragraph. However, for **3**, the values of the mixing functions were unequal for some of the special values of ϕ, ϕ' and the molecular symmetry possible for these special values of ϕ, ϕ' was necessarily lost. In the above example, the loss of symmetry occurs in two related ways: either $d(\phi, \phi') > d'(\phi, \phi')$ or $d(\phi, \phi') > d(\phi', \phi)$. The two-dimensional surface $E(\phi, \phi')$ is no longer unequivocal and has to be replaced by an explicit form containing those $d_i(\phi, \phi')$ and $\alpha_j(\phi, \phi')$ that mix under a given transformation of the ϕ's and that are unequal for special values of ϕ, ϕ'. The new function E depends on more variables and will be correspondingly more complicated. Thus, in the case of **3**, a more detailed analysis of the PE surface will be necessary.

The coordinates ϕ and ϕ' used repeatedly in the above discussion to describe an arbitrary conformation will now be defined in terms of the torsion angles ω_1, ω_2, ω_3 associated with one rotor and ω_4, ω_5, ω_6 associated with the other; ω_1 and ω_4 are the torsion angles defined by X(1)–C(1)–C(2)–C(3) and X(4)–C(3)–C(2)–C(1), respectively. Sketch B shows the structure and a schematic projection in which H(a) and H(b) point toward the observer and in which the CX_3 groups are viewed from C(2) toward C(1) and C(3). The other ω's are defined similarly. We define

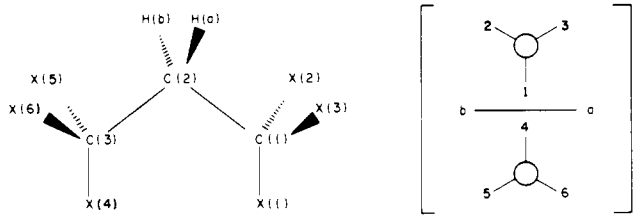

B

$$\phi = (\omega_1 + \omega_2 + \omega_3 - 2\pi)/3 \quad (1)$$

$$\phi' = (\omega_4 + \omega_5 + \omega_6 - 2\pi)/3 \quad (2)$$

where $0 \leq \omega_1 < 2\pi$ and $\omega_1 < \omega_2 < \omega_3$, with similar constraints for ω_4, ω_5, and ω_6. For conformation B, $\omega_1 = \omega_4 = 0$.

The functions $E(\phi, \phi')$ for **1** and **2** were obtained from EFF calculations. For each point (x, y), all other $3N - 8$ degrees of freedom were optimized to arrive at the corresponding conformation of minimum energy; this implies that $E(\phi, \phi')$ implicitly takes into account variations in d_i and α_j. For **3**, the calculations showed that two extra variables have to be taken into account. In view of the four-dimensional nature of the problem, only parts of E were determined, mostly in the neighborhood of the chemically important reaction pathways.

For **1** and **2**, an analytical representation of $E(\phi, \phi')$, which is invariant under the operations of $c2mm$ 3^2 (p), was chosen in terms of a double Fourier series

$$E(\phi,\phi') = \sum_{i=0}^{\infty}\sum_{j=0}^{\infty}(A_{ij}(\cos 3i\phi \cos 3j\phi') + B_{ij}(\sin 3i\phi \sin 3j\phi')) \quad (3)$$

(29) For the concept of *groups by modulus*, see: Shubnikov, A. V.; Koptsik, V. A. "Symmetry in Science and Art"; Plenum Press: New York, 1974; p 246.

(30) International Tables for X-ray Crystallography, Kynoch Press: Birmingham, England, 1969; Vol I, p 64.

(31) The first and second m represent mirror lines with positive and negative slopes, respectively. The 2 represents twofold rotational symmetry at the origin (0, 0) and at $(0, 2\pi/6)$, and the c represents a centered lattice.

(32) The standard representation of cmm in ref 30 is in terms of a centered unit cell with coordinates $(\phi + \phi')$, $(\phi - \phi')$, parallel to the mirror lines, translation distances $\sqrt{2}\,2\pi/3$, $\sqrt{2}\,2\pi/3$, and lattice points at 0, 0 and $^1/_2$, $^1/_2$. We prefer the nonstandard description in terms of a primitive unit cell with translation distances $2\pi/3$, $2\pi/3$ and diagonal mirror lines as in Figure 1B.

Table III. Stationary Points for the MM2 Hypersurface of Propane (1)[a]

ϕ	ϕ'	relative steric energy	type	molecular symmetry
60.000	60.000	0.000[b]	GS	$C_{2v}(2/2)$
60.000	0.000	3.036	TS	$C_s(2/1)$
0.000	0.000	6.597	M(2)	$C_{2v}(1/1)$

[a] Torsion angles (ϕ, ϕ') in degrees. Energies in kcal mol^{-1}. Type of point: GS = ground state, TS = transition state, M(n) = maximum with n negative eigenvalues (n = 0 and 1 for GS and TS, respectively). Where more than one isometric structure exists, only one representative is shown. [b] Absolute steric energy = 1.500 kcal mol^{-1}.

where $A_{ij} = A_{ji}$ and $B_{ij} = B_{ji}$. The coefficients A_{ij} and B_{ij} were determined by fitting eq 3 to a sufficient number of data points derived from EFF calculations. The series was truncated after the addition of further terms produced negligible changes in the second derivative matrix ($\partial^2 E/\partial\phi^2$) at stationary points.

Given the PE surface, trajectories were determined that connect the minima through transition states. For 1 and **2**, the method of Müller[33] was applied to the fitted surface. For **3**, the trajectories were obtained by initially distorting the transition-state structure along the transition vector[34] and then performing an unconstrained geometry optimization, starting with steepest descent and concluding with Newton–Raphson. The trajectories allow direct visualization of the reaction paths followed during conformational interconversion.

Empirical Force Field Calculations. Initially, EFF calculations were performed with the program BIGSTRN-2[35] and the MM2[36] force field for 1 and **2**[37] and the AM force field[40,41] for **3**.[4] The method of variable metric optimization was excellent for locating stationary points, but it failed to converge satisfactorily for constrained optimizations. Also, for a given stationary point, the number of zero and negative eigenvalues of the final, approximate inverse second-derivative matrix depended on the starting geometry. We therefore could not properly distinguish minima from partial maxima. To surmount these obstacles, we resorted to the Newton–Raphson optimization method, as implemented in the program BIGSTRN-3.[42] This program, derived from BIGSTRN-2, utilizes analytical first and second derivatives of the energy for the full matrix Newton–Raphson geometry optimization. All results reported here are based on the force field in Allinger's MM2 program.[44]

Calculations were performed in two steps. The first involved location of the stationary points on the hypersurface by unconstrained geometry optimization of the appropriate input structures[45] and calculation of the normal modes and vibrational frequencies for all stationary points. Conformations corresponding to partial maxima were distorted along the eigenvectors associated with negative eigenvalues and reoptimized to locate potentially new stationary points.[46] In the second step, calculations were made with one ω from each rotor constrained at preset values,[47] while optimizing all other internal parameters, in order to obtain additional nonstationary points[48] for the surface fitting. All optimizations were begun with steepest descent and concluded with Newton–Raphson; they were considered converged when the root-mean-square value of the first derivative of the energy was less than 10^{-6} kcal mol^{-1} Å^{-1} and root-mean-square value of the atom movement was less than 10^{-6} Å.

In the evaluation of the PE's, it should be kept in mind that EFF results refer to isolated molecules in a hypothetical, motionless state at 0 K.[41] However, the relative steric energies calculated for 1–**3** are presumed to approximate free energies ΔG or $\Delta G^{\ddagger}$ closely because entropy effects are expected to be negligible and zero-point energies of different conformers are believed to be closely comparable.

Table IV. Coefficients for Eq 3 Derived from EFF Results for Propane (1)[a]

$j\backslash i$	0	1	2	3
		$A_{ij} \times 10^2$		
0	472.560	165.585	−3.042 10	−0.490 395
1		13.3375	−0.239 058	−0.109 023
2			0.381 869	0.216 433
3				0.043 4500
		$B_{ij} \times 10^2$		
0	0	0	0	0
1		−3.180 77	0.985 821	−0.068 8028
2			0.016 5784	−0.075 3569
3				−0.045 0952

[a] In kcal mol^{-1}. Root-mean-square relative error is 0.076%.

Table V. Stationary Points for the MM2 Hypersurface of Di-*tert*-butylmethane (2)[a]

ϕ	ϕ'	relative steric energy	type	molecular symmetry
46.452	46.452	0.000[b]	GS	C_2
60.000	60.000	0.721	TS	$C_{2v}(2/2)$
60.000	0.000	4.859	TS	$C_s(2/1)$
0.000	0.000	11.375	M(2)	$C_{2v}(1/1)$

[a] See footnote *a*, Table III. [b] Absolute steric energy = 12.792.

Table VI. Coefficients for Eq 3 Derived from EFF Results for Di-*tert*-butylmethane (2)[a]

$j\backslash i$	0	1	2	3
		A_{ij}		
0	17.4675	2.801 33	0.135 665	−0.011 3104
1		0.761 276	−0.018 4099	−0.025 7182
2			0.510 661	−0.129 255
				−0.128 084
		B_{ij}		
0	0	0	0	0
1		−0.361 825	0.135 555	0.042 4277
2			−0.467 074	0.146 929
3				0.119 141

[a] In kcal mol^{-1}. Root-mean-square relative error is 0.50%.

Description of Hypersurfaces

Propane (1). Stationary points and relative energies are listed in Table III and coefficients A_{ij} and B_{ij} (eq 3) in Table IV. The torsional PE hypersurface is shown in Figure 2.

In the ground state, **1** assumes a $C_{2v}(2/2)$ conformation (i.e., a conformation with two methyl hydrogens on each rotor in "gear-clashed" opposition). The $C_s(2/1)$ "geared" conformation

(33) Müller, K. *Angew. Chem., Int. Ed. Engl.* **1980**, *19*, 1.
(34) Stanton, R. E.; McIver, J. W., Jr. *J. Am. Chem. Soc.* **1975**, *97*, 3632. Ermer, O. *Ibid.* **1976**, *98*, 3964.
(35) Iverson, D. J.; Mislow, K. *QCPE* **1981**, *13*, 410.
(36) Allinger, N. L. *J. Am. Chem. Soc.* **1977**, *99*, 8127.
(37) The stationary structures of **1** and **2** were also determined by use of the Allinger 1971[38] and MM1[39] force fields, with results essentially identical with those obtained with the MM2 force field.
(38) Allinger, N. L.; Tribble, M. T.; Miller, M. A.; Wertz, D. H. *J. Am. Chem. Soc.* **1971**, *93*, 1637.
(39) Wertz, D. H.; Allinger, N. L. *Tetrahedron* **1974**, *30*, 1579.
(40) Andose, J. D.; Mislow, K. *J. Am. Chem. Soc.* **1974**, *96*, 2168.
(41) Mislow, K.; Dougherty, D. A.; Hounshell, W. D. *Bull. Soc. Chim. Belg.* **1978**, *87*, 555 and references therein.
(42) The program BIGSTRN-3 is being prepared for submission to QCPE. A listing is available upon request. The program uses full matrix Newton–Raphson optimization. All atoms are moved simultaneously, and symmetry is thus conserved. For a critical discussion of symmetry conservation during geometry optimization, see Ermer.[43]
(43) Ermer, O. *Tetrahedron* **1975**, *31*, 1849.
(44) Allinger, N. L.; Yuh, Y. H. *QCPE* **1981**, *13*, 395. There are slight differences between the parameters found in this program and those reported in the original reference[36] to MM2. We opted to use those in the Allinger–Yuh program, with two modifications designed for C_{ar}–C_{ar} bonds (l^0 = 1.3937 Å and k_s = 8.0667 mdyn Å^{-1}). See also: Ōsawa, E.; Onuki, Y.; Mislow, K. *J. Am. Chem. Soc.* **1981**, *103*, 7475.
(45) The input structures for the stationary points had symmetry higher than C_1: C_{2v} (0, 0), C_{2v} (60°, 60°), C_2 (30°, 30°), C_s (0, 60°). In all calculations for **2**, the input geometries for the methyl groups were staggered; eclipsed conformations were not investigated.
(46) This technique avoids the problem inherent in other methods of mistaking partial maxima for minima, and also does not require point-by-point mapping of reaction paths (thus, the risky "group driving" technique can be avoided).[43] See also: Ermer, O. "Aspekte von Kraftfeldrechnungen"; Wolfgang Baur Verlag: Munich, 1981.
(47) A harmonic restoring potential ($E = 0.5k(\omega - \omega_0)^2$) was applied to fix the internal coordinate ω at the prescribed value ω_0 ($k = 10^5$ kcal mol^{-1} rad^{-1}).
(48) Input structures for general (nonstationary) points on the hypersurface had the following symmetries: $C_1(x, y)$, $C_2(x, x)$, $C_s(x, -x)$. Multiples of 15° were used as values for ω_0.[47]

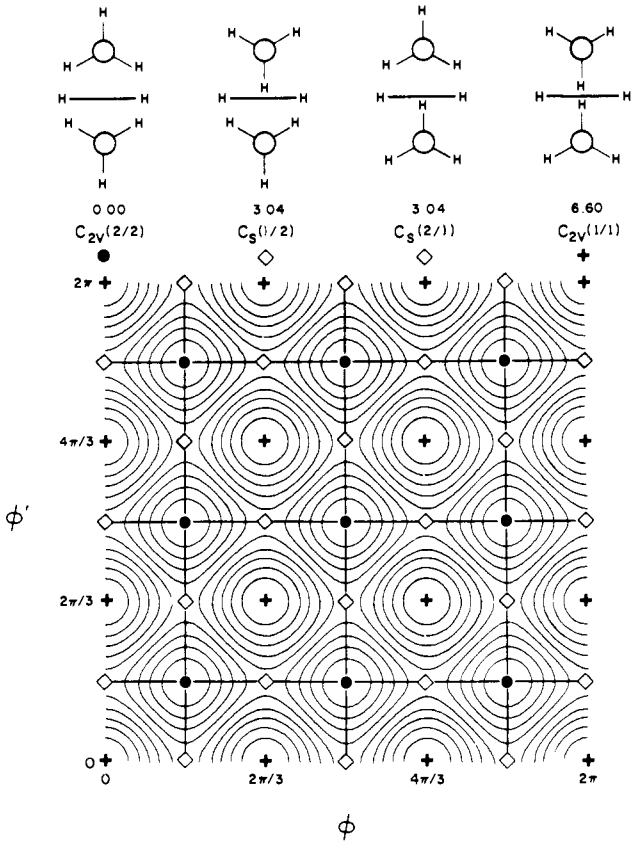

Figure 2. (Top) Schematic projections of the stationary structures of propane (1), following the convention for structure B (see text), with relative steric energies (in kcal mol^{-1}), symmetries, and mapping symbols. (Bottom) Contour map of the torsional PE hypersurface for 1. Stationary points correspond to the structures shown on top. Contour intervals are at 0.66 kcal mol^{-1}. Heavy lines indicate minimum-energy trajectories interconnecting ground states.

is a transition state 3.04 kcal mol^{-1} above the ground state, and the $C_{2v}(1/1)$ "gear-clashed" conformation a double partial maximum (hilltop).[49] The minimum-energy pathways by way of the C_s conformation clearly show that the torsion of the two methyl rotors is uncorrelated, i.e., each methyl group rotates independently of the other. Thus, a single process interconverts all nine isometric structures (Table II).

Superficially, the hypersurface appears to have fourfold symmetry (plane group *p4m*), and the trajectories appear to be straight lines. However, if this were the case, all B_{ij}'s would vanish, contrary to calculation (Table IV). The small but not insignificant values of these coefficients ensure that the symmetry of the hypersurface remains isomorphic only to *cmm*. This symmetry does not require the trajectories to be straight lines (as would be the case for *p4m*), and the deviation from linearity is borne out by a close examination of the normal modes of the stationary structures.[51]

There have been several reports on the barrier to rotation and on torsional potential constants for propane on the basis of experimental data[8e,k,t] and MO calculations.[8r,u] The reported barriers range from 3.110 to 3.400 kcal mol^{-1}, and our calculated barrier of 3.036 kcal mol^{-1} is judged to be in good agreement. Our calculated values of A_{10} and A_{11} are also in good agreement with published values, but B_{11} is about two orders of magnitude smaller than previously reported. We believe it likely that this discrepancy is due to the standard geometries and to the rigid rotor approximation used by the previous workers.

(49) The anisometry of the two C_{2v} conformations of **1** is an example of the failure of point group specification, which is an "unduly coarse method of conveying symmetry information."[50] Pople's classification by framework groups[50] also fails to discriminate between these structures, since $C_{2v}(2/2)$ and $C_{2v}(1/1)$ both belong to C_{2v} [C_2(C), σ_v(H_2), σ_v'($(CH)_2$), X(H_4)]. Standard space group nomenclature avoids this type of ambiguity by assigning different Wyckoff symbols to different special positions some of which may show the same site symmetry (cf. ref 30).

(50) Pople, J. A. *J. Am. Chem. Soc.* **1980**, *102*, 4615. See also: Flurry, R. L., Jr. *Ibid.* **1981**, *103*, 2901.

(51) If the symmetry were *p4m*, the vibrational frequencies of the two torsional modes for the stationary structures of **1** would have to be equal, contrary to calculation. Furthermore, the eigenvector at the transition state would show a contribution from only one methyl torsion, also contrary to calculation.

Table VII. Stationary Points for the MM2 Hypersurface of Bis(9-triptycyl)methane (3)[a]

ϕ	ϕ'	relative steric energy	type	molecular symmetry
32.110	32.110	0.000[b]	GS	C_2
60.000	0.000	0.185	TS	$C_s(2/1)$
60.000	60.000	30.094	TS	$C_s(2/2)$
60.000	60.000	~61	M(4)[c]	$C_{2v}(2/2)$
0.000	0.000	~75	M(5)[c]	$C_{2v}(1/1)$

[a] See footnote *a*, Table III. [b] Absolute steric energy = 41.6587. [c] The geometry optimization for this partial maximum did not converge but oscillated around this structure. The oscillation appears to be due to spontaneous desymmetrization toward a $C_s(n/n)$ conformation.

Table VIII. Selected Structural Parameters for Stationary Points of Bis(9-triptycyl)methane (3)[a]

parameter	C_2	$C_s(2/1)$	$C_s(2/2)$	$C_{2v}(2/2)$	$C_{2v}(1/1)$
d[b]	1.554	1.542	1.580	1.716	1.693
d'	1.554	1.566	1.553	1.716	1.693
α_{CCC}[c]	130.2	129.4	137.1	150.5	148.9
α_{XCX}[d]	99.7	100.6	104.9	96.9	96.6
	102.8	100.6	104.9	96.9	96.6
	103.8	106.7	91.7	100.5	100.4
$\alpha_{XCX'}$	102.8	101.9	93.6	96.9	96.6
	103.8	101.9	93.6	96.9	96.6
	99.7	101.1	115.8	100.5	100.4

[a] In each set of parameters, primed and unprimed values refer to the rotors with torsion angles ϕ' and ϕ, respectively. [b] Central C–C bond lengths in angstroms. [c] Central C–CH_2–C bond angle in degrees. [d] X–C–X bond angles (see sketch B, text) in degrees.

Di-*tert*-butylmethane (2). Stationary points and relative energies are listed in Table V and coefficients A_{ij} and B_{ij} in Table VI. The torsional PE hypersurface is shown in Figure 3.

In the ground state, **2** assumes a chiral C_2 conformation, with a calculated central C–CH_2–C bond angle of 124.3° and a *tert*-butyl torsion angle $\phi = \phi' = 46.5°$, in good agreement with experiment[12] and with previous EFF calculations.[12,13e] Two anisometric, achiral transition states were located within a $(2\pi/3) \times (2\pi/3)$ unit cell, one with a $C_{2v}(2/2)$ and the other with a $C_s(2/1)$ conformation. In addition, the unit cell contains a partial maximum with $C_{2v}(1/1)$ symmetry. In contrast to Figure 2, the symmetry of the surface in Figure 3 (*c2mm* 3^2 (p)) is obvious by inspection. See also Table II.

There are two nonequivalent pathways, both of which interconnect enantiomers. One of these (a $\rightleftarrows$ b, Figure 3) requires a barrier of merely 0.72 kcal mol^{-1} and passes through the transition state with $C_{2v}(2/2)$ symmetry. The other (a $\rightleftarrows$ c, Figure 3) requires a barrier of 4.86 kcal mol^{-1} and passes through the transition state with $C_s(2/1)$ symmetry. In the former, C_2 symmetry is maintained throughout (the trajectory lies along a mirror line) and the two *tert*-butyl rotors therefore undergo conrotation to the same extent. In the latter, C_2 symmetry is destroyed and the two rotors undergo disrotation to different degrees.

Both pathways involve correlated rotation of the rotors. However, *combination* of the two (c $\rightleftarrows$ a $\rightleftarrows$ b, Figure 3) results in overall homomerization with net uncorrelated rotation (in the example, the *net* motion of one rotor is $2\pi/3$ while that of the other is 0). In contrast, the pathway $c \rightleftarrows a \rightleftarrows d$ (Figure 3), which has the identical energy requirement as the other composite pathway, also leads to homomerization, but with net disrotation (in the example, both rotors move by $2\pi/3$, but in opposite directions). Therefore the two composite processes just described

Table IX. Selected Structural Parameters for Bis(9-triptycyl)methane (3) for Gearing and Gear-Slippage Pathways[a]

ω_1	ω_2	ω_3	ϕ	r	θ	ω_4	ω_5	ω_6	ϕ'	r'	θ'	relative energy
						Gearing Pathway						
63.7	180.0	296.3	60.0	5.26	60.0	0.0	122.7	237.3	0.0	3.86	0.0	0.185
54.2	173.2	287.2	51.5	5.36	37.9	10.7	133.6	247.6	10.6	4.24	0.8	0.121
50.0	169.9	283.4	47.7	5.45	30.7	15.4	138.4	251.9	15.2	4.56	2.4	0.095
43.5	164.5	277.3	41.8	5.50	23.2	22.5	145.3	258.2	22.0	5.03	6.5	0.044
40.6	161.9	274.6	39.0	5.49	20.4	25.6	148.3	261.0	25.0	5.20	8.6	0.013
35.6	157.5	270.1	34.4	5.45	16.2	30.7	153.0	265.6	29.8	5.36	12.3	0.001
33.2	155.3	267.9	32.1	5.41	14.2	33.2	155.3	267.9	32.1	5.41	14.2	0.000
						Gear-Slippage Pathway						
61.6	180.0	298.4	60.0	2.31	60.0	70.2	180.0	289.8	60.0	14.39	60.0	30.094
50.2	170.0	286.8	49.0	2.64	32.9	75.5	184.9	295.2	65.2	14.35	61.3	29.695
42.8	163.6	279.5	42.0	3.05	19.8	78.5	188.0	298.7	68.4	14.03	62.2	29.112
35.8	157.4	272.5	35.2	3.51	11.0	81.0	190.6	302.0	71.2	13.44	63.0	27.912
28.2	151.2	265.6	28.5	3.95	4.3	83.0	192.9	305.0	73.6	12.75	63.8	26.298
17.9	141.5	255.2	18.2	4.48	−3.9	85.1	195.9	308.9	76.7	11.53	64.3	22.397
10.8	135.0	248.4	11.4	4.72	−8.5	85.3	197.0	310.3	77.5	10.59	63.6	18.089
4.1	129.1	242.4	5.2	4.95	−16.0	81.9	195.3	309.0	75.4	9.15	60.6	10.481
0.9	126.5	239.9	2.4	5.02	−21.4	74.6	189.9	304.1	69.6	7.39	56.5	3.777
2.5	125.7	240.1	2.8	4.00	−4.3	62.4	179.4	294.8	58.9	5.39	52.7	0.211
33.2	155.3	267.9	32.1	5.41	14.2	33.2	155.3	267.9	32.1	5.41	14.2	0.000

[a] First and last entries in each set (gearing and gear-slippage pathways) are transition- and ground-state structures, respectively. Angles (ω, ϕ, r, and θ) in degrees, energy in kcal mol^{-1}.

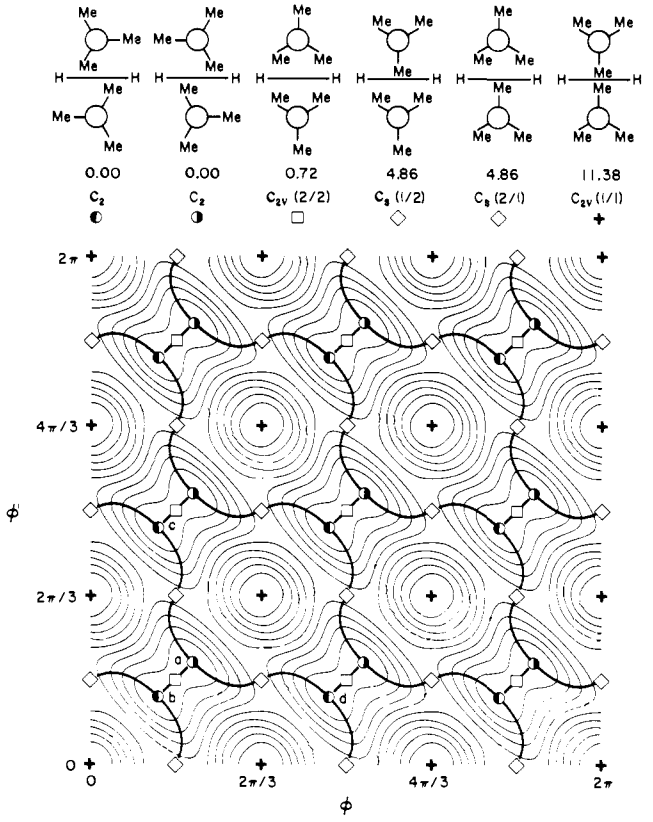

Figure 3. (Top) Schematic projections of the stationary structures of di-*tert*-butylmethane (**2**), following the convention for structure B (see text), with relative steric energies (in kcal mol^{-1}), symmetries, and mapping symbols. (Bottom) Contour map of the torsional PE hypersurface for **2**. Stationary points correspond to the structures shown on top. Contour intervals are at 1.14 kcal mol^{-1}. Heavy lines indicate minimum-energy trajectories interconnecting ground states.

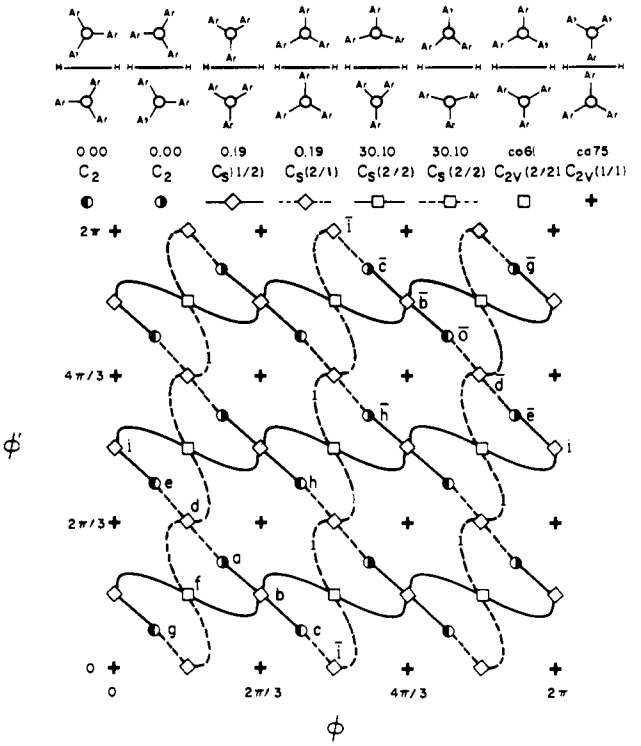

Figure 4. (Top) Schematic projections of the stationary structures of bis(9-triptycyl)methane (**3**), following the convention for structure B (see text), with relative steric energies (in kcal mol^{-1}), symmetries, and mapping symbols. Distortions in the $C_s(2/2)$ projections are exaggerated for clarity. (Bottom) Map of trajectories for **3**. Stationary points correspond to the structures shown on top. Solid lines indicate minimum-energy trajectories above the plane of projection interconnecting ground states in the plane of projection. Dashed lines indicate trajectories below the plane of projection.

will interconvert all 18 isometric structures that correspond to special positions (Table II).[52]

Bis(9-triptycyl)methane (3). Stationary points and relative energies are listed in Table VII and selected structural parameters in Table VIII. Trajectories on the torsional PE hypersurface are shown in Figure 4, and selected structural parameters are listed in Table IX.

Like **2**, **3** assumes a chiral C_2 conformation in the ground state, with a calculated central C–CH_2–C bond angle of 130.2° and calculated 9-triptycyl (Tp) torsion angles $\phi = \phi' = 32.1°$.[53] Four

(52) The methyl groups do not perform a full $2\pi/3$ rotation during these interconversion processes but merely oscillate a little around their equilibrium positions.

(53) Preliminary calculations[4] using BIGSTRN-2[35] in conjunction with the AM force field[40] had indicated a $C_s(2/1)$ ground state for **3** and a gearing transition state with C_2 symmetry lying ca. 1.0 kcal mol^{-1} above the ground state.

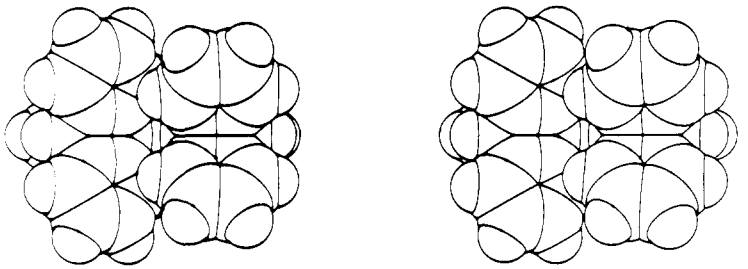

Figure 5. A stereoview of the calculated $C_s(2/2)$ gear-slippage transition state for bis(9-triptycyl)methane (**3**). The view is along the bisector of the central C–CH_2–C bond angle, with the methylene hydrogens distal to the observer.

achiral transition states were located in the $(2\pi/3) \times (2\pi/3)$ unit cell. Two of these, an isometric pair, lie 0.19 kcal mol^{-1} above the ground state and show a $C_s(2/1)$ conformation similar to that found for **2**.[54] The other two, another isometric pair, are related to the $C_{2v}(2/2)$ transition state of **2** but show an additional strong desymmetrization, which makes an explicit description outside the parameter space ϕ, ϕ' unavoidable. These transition state structures may be described as $C_s(2/2)$ conformations; in each, two benzene rings within one Tp moiety are squeezed together and tucked into the notch between two rings in the other (see Figure 4, top, and Figure 5). Their energy is 30.1 kcal mol^{-1} above the ground state. The $C_{2v}(2/2)$ conformation in the ϕ, ϕ' plane lacking this type of deformation corresponds to a fourfold partial maximum ca. 61 kcal mol^{-1} above the ground state. In addition, there is a partial maximum with $C_{2v}(1/1)$ symmetry, ca. 75 kcal mol^{-1} above the ground state.

The PE surface for **3** is significantly more complex than that for **2**, largely because of the existence of the two isometric $C_s(2/2)$ transition states at $(\phi, \phi') = ((\pi/3) + (n2\pi/3), (\pi/3) + (n'2\pi/3))$. As we shall show below, this makes it necessary to introduce at least two extra dimensions into the description of the PE surface. A four-dimensional representation is difficult to visualize, and we can therefore not draw contour diagrams as for **1** and **2**. Instead, we have chosen to tabulate ω_i's along the calculated reaction paths (Table IX) and to give a graphical representation of the network of minima, transition states, and interconnecting pathways (Figure 4).

The $C_s(2/2)$ transition states show severe distortion of the molecule from C_{2v} symmetry and of the rotors from local C_{3v} symmetry. To describe these in terms of ω_i's, we proceed as follows: the six CCCX torsion angles ω_i about the two central bonds in B can be used to generate six independent symmetry distortion[25] coordinates that transform as A_2, A_3, and G irreducible representations of G_{36}. The two one-dimensional A_2 and A_3 coordinates S_1 and S_2 are linear combinations of ϕ and ϕ' (eq 4 and

$$S_1 = (\phi + \phi')/\sqrt{2} \quad (4)$$

$$S_2 = (\phi - \phi')/\sqrt{2} \quad (5)$$

5) and represent con- and disrotation, respectively. The remaining four coordinates belong to the four-dimensional representation G and are given in eq 6–9. The quantities S_{3a} and S_{3b} describe

$$S_{3a} = (2\omega_1 - \omega_2 - \omega_3 + 2\pi)/\sqrt{6} \quad (6)$$

$$S_{3b} = (\omega_2 - \omega_3 + (2\pi/3))/\sqrt{2} \quad (7)$$

$$S_{3c} = (2\omega_4 - \omega_5 - \omega_6 + 2\pi)/\sqrt{6} \quad (8)$$

$$S_{3d} = (\omega_6 - \omega_5 + (2\pi/3))/\sqrt{2} \quad (9)$$

distortions of one rotor from local C_{3v} symmetry, while S_{3c} and

Scheme I

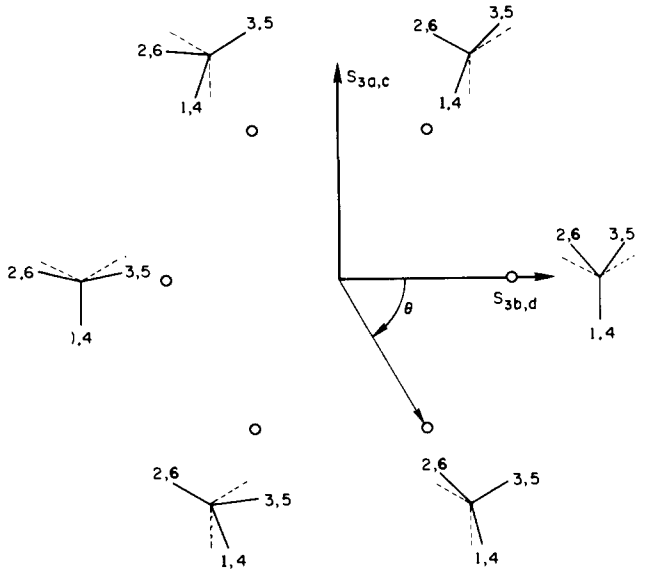

S_{3d} describe distortions of the other. The distortion coordinates of each rotor can be transformed into polar coordinates, r, θ, where

$$r = (S_{3a}^2 + S_{3b}^2)^{1/2} \qquad r' = (S_{3c}^2 + S_{3d}^2)^{1/2}$$

$$\theta = \arctan(S_{3a}/S_{3b}) \qquad \theta' = \arctan(S_{3c}/S_{3d})$$

Here, the r's measure the degree by which the differences between consecutive ω_i's deviate from 120°, and the θ's indicate where the deviations are mainly localized (Scheme I and Table IX).

As a next step, we have to ask how the r's and θ's transform if we transform ϕ, ϕ' using an operation of *c2mm* 3^2 (p). With x, y, s, t, u, v as the components along the coordinate axes ϕ, ϕ', θ, θ', r, r', respectively, we obtained the following transformation: $(-x, -y, -s, -t, u, v)$, (y, x, t, s, v, u), $(x + (2\pi/3), y, s + (2\pi/3), t, u, v)$, and $(x, y + (2\pi/3), s, t + (2\pi/3), u, v)$ (we only list the generators for the six-dimensional representation of the molecular symmetry group in the space ϕ, ϕ', θ, θ', r, r'). Note that for $x = y$, $x = -y$, etc., u would have to equal v if the molecular symmetries associated with special values of ϕ, ϕ' were to be preserved (Table II), whereas in actual fact u and v are unequal for $x = y = 60°$, and therefore the molecular symmetry is only C_s rather than the maximally possible C_{2v} (Table VII). The advantage of r, r', θ, θ' over the ω_i's is that the functions $r(\phi, \phi')$, $r'(\phi, \phi')$ pertinent to the reaction network are periodic in ϕ and ϕ' with periods $2\pi/3$ and are always positive. The functions $\theta(\phi, \phi')$, $\theta'(\phi, \phi')$ have values between 0 and 2π, but again these values are periodic in ϕ, ϕ' with period 2π. The transformation properties are the same as those for ϕ, ϕ'.

A brief consideration of the numerical values of r, r', θ, θ' (Table IX) in the rearrangement network of **3** will be necessary before we proceed to a discussion of Figure 4. The values of r and r', which are 5.4° at the C_2 minima, change very little on going to the $C_s(2/1)$ transition state. However, $r = 2.3°$ and $r' = 14.4°$ for the $C_s(2/2)$ transition state, and all along the pathway that traverses this point (solid lines, Figure 4), r remains small

(54) The molecular structure of **3** in the crystal[55] is asymmetric, but the values for ϕ, ϕ', and the central C–CH_2–C bond angle (50.2, 9.9, and 129.3°, respectively) deviate only slightly from the corresponding values for the calculated $C_s(2/1)$ structure (60.0, 0.0, and 129.4°, respectively). This finding is consistent with the calculated small energy difference between C_2 ground and $C_s(2/1)$ transition states.

(55) Johnson, C. A.; Guenzi, A.; Nachbar, R. B., Jr.; Blount, J. F.; Wennerström, O.; Mislow, K. *J. Am. Chem. Soc.* **1982**, *104*, 5163.

(2.3–5.4°) while r' varies from 5.4 to 14.4°. Throughout the high-energy portion of this trajectory (3.8–30.1 kcal mol^{-1}), θ' remains approximately constant to within ±5° at 60, 180, or 300° for ranges of ϕ' of 43–77°, 163–197°, or 383–317°, respectively. Conversely, r = 14.4° and r' = 2.3° for the $C_s(2/2)$ transition state that lies on the dashed trajectory; there is now little variation in r' while r varies from 5.4 to 14.4° and θ remains approximately constant. Thus, the solid lines in Figure 4 express the fact that one rotor (ω_4, ω_5, ω_6) shows severe distortion from local C_{3v} symmetry, whereas the other one does not. Any transformations of the ϕ's that take a solid line into a dashed line also take the distortion from one rotor to the other. Thus Figure 4 is at best pseudo-three-dimensional. The coordinate θ' pointing from the plane of projection (ϕ, ϕ') toward the observer is actually different from and orthogonal to the coordinate θ pointing away from the plane (ϕ, ϕ'). The solid and dashed lines in Figure 4 serve as a reminder: if ϕ and ϕ' are transformed, θ and θ' must be transformed accordingly.

Gearing and Gear Slippage in Bis(9-triptycyl)methane. Our calculations indicate that the Tp moieties in **3** undergo virtually unhindered yet strongly coupled disrotation. Thus, in the language of the mechanical analogy, **3** behaves as a tightly meshed and almost frictionless bevel gear system; the cogs are benzene rings that fit into the V-shaped notches formed by pairs of benzene rings in the other rotor. The gearing trajectories run along the bottoms of deep valleys on the PE hypersurface and connect the enantiomeric C_2 ground states via $C_s(2/1)$ transition states that are barely higher in energy. Thus, the PE hypersurface is virtually flat along the gearing coordinate. In Figure 4, the trajectories are indicated by slightly sinusoidal diagonal lines. Note that these lines in the projection plane are under no constraint to be linear, because they coincide with diagonal glide lines rather than mirror lines (Figure 1B). That is, the molecule does not have to maintain C_2 or C_s symmetry.

To describe the structural variations of **3** along the gearing pathway, consider the enantiomerization a → b → c (Figure 4). Torsional deformation of the C_2 ground state a leads to a $C_s(2/1)$ transition state b. The principal component of this motion on the hypersurface is, of course, S_2 (disrotation). There are, however, small contributions from S_1[56] (conrotation), r, r', θ, and θ'. The central bond lengths (d) and the central bond angle (α_{CCC}) change smoothly from a → b → c, but these structural variations along the gearing path are negligible compared to changes in ϕ and ϕ' (Table IX). Motion in the reverse direction, a → d → e, is symmetrically related to forward motion by the transformation (ϕ', ϕ, θ', θ, r', r) as described above.

A second process, which is also an enantiomerization, converts the C_2 ground state to its mirror image via a $C_s(2/2)$ transition state (f in Figure 4) 30.1 kcal mol^{-1} higher in energy. A molecule of **3** must initially disrotate (a → b) to reach this highly strained and distorted structure (Tables VII and VIII), but just before b is reached, a sharply increasing contribution from S_1 (conrotation) results in a → f. Descent from the transition state toward g is related to the ascent (a → f) by the transformation ($-\phi' + (2\pi/3)$, $-\phi + (2\pi/3)$, $-\theta' + (2\pi/3)$, $-\theta + (2\pi/3)$, r', r). Overall, the path a → f → g results in enantiomerization. Initial disrotation in the reverse direction, toward d, traces a path (a → g, dashed) below the plane of projection that is related to the above-described trajectory by the transformation ϕ', ϕ, θ', θ, r', r. The roles assumed by the two Tp moieties along the solid and dashed pathways are switched: thus the primed and unprimed values for d and α_{XCX} in Table VIII, which refer to structures along the solid pathway a → f → g, are reversed for the dashed pathway.

Because the net result of a → g is conrotation, i.e., gear slippage, one may wonder whether synchronous conrotation (pure S_1 rotation) is available to **3**. However, according to our calculations, this pathway requires the intermediacy of the grossly distorted $C_{2v}(2/2)$ structure (Table VIII) that corresponds to a partial maximum ca. 61 kcal mol^{-1} above the ground state (Table VII). This path may therefore be safely ruled out of consideration.

(56) In terms of the mechanical gear analogy, this contribution can be visualized as a measure of the play between the gears.

Labeling and Isomerism

General Considerations. Each interconversion between isometric conformations corresponds to a symmetry operation, permutation, or matrix transformation; i.e., there are as many interconversions as there are symmetry operations in the MSG. However, for conformations with nontrivial covering (point group) symmetry (e.g., C_{2v} for **1** and C_2 for **2** and **3**), certain sets of these interconversions (symmetry operations) become indistinguishable;[18] such sets are known as rearrangement modes. Group theoretically, these modes are obtained by evaluating the double cosets PgP, where $g \in G_{36}$, and P is the covering symmetry group of order p.[17] For **1**, with $P = C_{2v}$, there are only 4 different double cosets, and for **2** and **3**, with $P = C_2$, there are 12 different double cosets. The operations in a double coset generate a group G_i of order i, which is a subgroup of G_{36}[57] and which represents the apparent symmetry of the molecule under the operations of given modes on the time scale of observation. The operations of this subgroup applied to a reference conformation will interconvert it with $n = i/p$ isometric conformations but not with the others. The isometric structures are thus partitioned into $Z = N/n$ disjoint sets, where N is the number of isometric structures with covering symmetry P (see Table II). The Z disjoint sets are indistinguishable; that is, there is a one-to-one correspondence between the elements for each pair of sets.

We illustrate these somewhat abstract group theoretical results by considering the case of **3**. As shown by the EFF calculations, the equilibrium conformation has C_2 symmetry, leaving 12 different rearrangement modes (double cosets); we assume that chemical realizations of these modes are possible only along the reaction pathways obtained from the EFF calculations.[58]

For the isomer a in Figure 4, enantiomerizations to c or e are the only primitive rearrangement processes[59] possible under ordinary laboratory conditions. The corresponding operations are ($-x - (2\pi/3)$, $-y + (2\pi/3)$) and ($-x + (2\pi/3)$, $-y - (2\pi/3)$) (23 and 19 in Table I); they belong to the same double coset since $C_2 \times 23 \times C_2 = \{19, 23\}$ ($C_2 = \{1, 10\}$ in Table I). In terms of Figure 4, we see that a lies on a special position, the positive mirror line, and that the enantiomerization pathways to c and e are transformed into each other by just this mirror line.[60] The double coset {19, 23} generates a group G_{12} whose operations interconvert a with c, c̄, ā, ē, and e (the order in which these structures are encountered on the gearing pathway, Figure 4). The number n of members of this set is 12/2 = 6. There are 18 isometric C_2 conformations in the $2\pi \times 2\pi$ space shown in Figure 4 (Table II): six of these constitute the set just described, and two more sets can be derived from reference conformations h and h̄, respectively (Figure 4). The 18 C_2 conformations are thus partitioned into $Z = 18/6 = 3$ indistinguishable sets of six each. Under ordinary laboratory conditions the conformers *within* each set undergo rapid interconversion under the operation of the gearing mode (Figure 6), but there is no interconversion *between* sets, since the gearing valleys are separated by high-energy ridges, with the lowest pass at f. Thus, though the three sets are indistinguishable, they are not interconvertible.

Labeling. The degeneracy between the three sets can be lifted by desymmetrization, achievable by appropriate chemical labeling of the ligands that occupy the sites in A (for example, the benzene rings in **3**). In choosing labels, we have to observe two conditions: first, the label should not modify the PE hypersurface to any significant extent, and second, the label should provoke a significant change in an observable quantity not directly related to

(57) Two modes generate the same group if one contains inverses of the elements in the other.

(58) We exclude tunneling, rearrangements making use of excited state surfaces, etc.

(59) A primitive rearrangement process connects an energy minimum across a single rate-determining transition state with the neighboring minimum.

(60) This result is general; primitive or nonprimitive rearrangement processes related by the covering symmetry of the starting conformation belong to the same rearrangement mode (double coset).

energy. If this procedure is followed, it may be safely assumed that the type and number of structures is still the same as for the unsubstituted molecule and that they interconvert within the same number of disjoint sets.[61] Carefully chosen labeling patterns (see below) will thus permit a distinction among the different disjoint labeled sets. Such a distinction may be one among stereoisomers; in the case of **3** at room temperature, it is one among residual stereoisomers, since each labeled set itself contains stereoisomers that undergo rapid interconversion under these conditions.[62]

Enumeration of Isomers. It remains to enumerate all types of residual stereoisomers resulting for every possible type of substitution pattern from the energetically feasible rearrangement modes. This enumeration is accomplished by counting the number of distinct double cosets $G_i g L_j$ ($g \in G_{36}$). Here, the group L_j of order j is the MSG of the labeled molecule; it is a subgroup of G_{36} and thus expresses the loss of molecular symmetry upon labeling. The corresponding matrix or space group[28] becomes a subgroup of $c2mm$ 3^2 (p). Systematic desymmetrization leads to eleven subsymmetries of the MSG. In Table X are listed the 12 L_j's, the corresponding matrix groups, and substitution patterns representative of each. Though numerous other substitution patterns are possible, the list of 12 L_j's exhausts the possibilities for symmetry dilution of G_{36}. For example, the patterns ABA-ABAAB or ACAABAAB are equally valid as alternatives for the representative pattern (AAABCABC) listed for L_{2c} in Table X: all such patterns are stereochemically correspondent.[63] The rearrangement mode groups G_i are restricted to those that are based on energetically feasible and chemically realistic primitive rearrangements,[59] as dictated by the EFF calculations that provide the information on the mechanistic and energetic aspects of the rearrangement processes.[64] These processes are associated with the following G_i's: G_{36} and G_{4b} for **1**; G_{36}, G_{12}, G_{4a}, and G_2 for **2** and **3** (Table X, footnote c). The five G_i's head the rightmost columns in Table X, the elements of which are the numbers of meso and DL isomers for each substitution pattern and rearrangement mode.[65,66] In what is to follow, we assume that the molecular ensemble is achiral and is observed under achiral conditions.

As an example, we discuss compound **3** with $G_i = G_{12}$ (gearing of the two Tp groups), $L_j = L_4$ (equal labeling of two phenyl rings, one in each Tp group) and the matrix group $c2mm$ 1^2 (p) with just one positive and one negative diagonal mirror and glide line, respectively, and four twofold rotation points in the $2\pi \times 2\pi$ unit cell (at {0, 0}, {0, π}, {π, 0}, and {π, π}). The operation of the left cosets gL_4 divides the 18 (formerly isometric) conformations that correspond to energy minima (◐, ◑ in Figure 4) into six sets of different isomers, namely {a, ā}, {h, h̄}, {g, ḡ}, {c, c̄, e, ē}, etc. The effect of operating with G_{12} on these sets follows from the previous section; i.e., the set {a, ā} interconverts exclusively with {c, c̄, e, ē}, {h, h̄} with {g, ḡ}, etc. The result is two sets, {a, ā, c, c̄, e, ē} and {g, ḡ, h, h̄, etc.}, corresponding to two different cosets obtained from $G_{12}\, g\, L_4$. The first set consists of interconverting enantiomers and is therefore achiral on the average (Figure 6, with 1 = 2 = A, 3 = B, 4 = 5 = A, 6 = B; see sketch C). We call this a meso

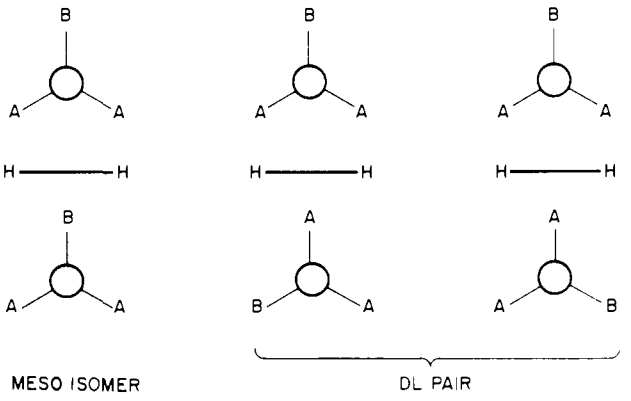

C

isomer. The second set consists of noninterconverting (under G_{12}) enantiomers: {g, h̄, etc.} on the one hand (Figure 6, with 1 = 2 = A, 3 = B, 4 = 6 = A, 5 = B; see sketch C) and {ḡ, h, etc.} on the other (Figure 6, with 1 = 2 = A, 3 = B, 5 = 6 = A, 4 = B; see sketch C). We call this a DL pair. In row L_4 and column G_{12} of Table X, we find the entry 1/1 for one meso isomer and one DL pair.

The other entries in Table X may be obtained from analogous reasoning. They make it possible to describe isomerism among the variously substituted derivatives of **1–3** under a variety of conditions. Thus, under conditions of rapid methyl rotation, the isomers of labeled propane derivatives are counted by using G_{36}: there will either be one meso species or one DL pair ($Z = 1$). This is the situation that obtains when the internal torsional motion proceeds along the minimum-energy pathway (see above), since G_{36} is the group generated from the double coset representing this motion. At the slow rotation limit (or under conditions of very fast observation), however, G_{4b} ($Z = 9$) becomes appropriate; that is, in a maximally labeled derivative,[67] one will now observe nine noninterconverting DL pairs.

For derivatives of **2**, appropriate G_i's for *tert*-butyl group rotation are G_{36} ($Z = 1$), G_{4a} ($Z = 9$), and G_2 ($Z = 18$), in order of decreasing time scales of observation. Under conditions where torsional motion is rapid through the $C_s(2/1)$ transition state (a ⇄ c, Figure 3), it is also rapid through the lower $C_{2v}(2/2)$ transition state (a ⇄ b, Figure 3). The G_i generated from the two double cosets representing each motion now applies; this is G_{36}, and one residual DL pair is thus expected for a maximally labeled structure. Finally, when both processes are frozen out, G_2 becomes applicable and 18 residual DL pairs remain, though this is unlikely to be realized given the magnitude (0.72 kcal mol^{-1}) of the lower barrier.[61,68]

(61) Strictly speaking, of course, $E(\phi, \phi')$ will have lower symmetry in the labeled case. However, under ideal conditions, the symmetry will remain approximately $c2mm$ 3^2. Such conditions are assumed throughout this discussion.

(62) Residual stereoisomerism results whenever closed subsets of appropriately substituted interconverting isomers are generated from the full set of isomers at a particular time scale of observation and under the operation of a given stereoisomerization mode.[19a]

(63) Gust, D.; Finocchiaro, P.; Mislow, K. *Proc. Natl. Acad. Sci. U.S.A.* **1973**, *70*, 3445. Nourse, J. G. *Ibid.* **1975**, *72*, 2385.

(64) A particular permutation only gives information relating to models of a given starting structure and the final structure that results from the rearrangement in question. It emphatically says nothing about the mechanism of the rearrangement it describes: no information pertaining to energetics or geometries of intermediate states traversed during a rearrangement is implied in, or may be inferred from, a permutation.

(65) As used in the present and previous[4] paper, the term "meso" refers to an isomer that is achiral by virtue of possession of an improper axis of rotation (S_n, including σ ($n = 1$) and i ($n = 2$)) or because any chiral components, referred to as *d* and *l* isomers, undergo rapid interconversion under the operation of the given rearrangement mode. In contradistinction, a "DL" pair consists of two residual enantiomers that are not interconverted under the operation of the mode and thus retain their individual chirality; by implication, the chiral components (*d* or *l*) do not enantiomerize under the operation of the mode.

(66) The isomer count was calculated from the number of isomers, Z_a and Z_c, in achiral and chiral environments, respectively. The number of meso and DL isomers is given by $2Z_a - Z_c$ and $Z_c - Z_a$, respectively. Z_a and Z_c in turn were evaluated by counting the number of double cosets AgL_j, where A is the group generated by the operational mode. For achiral environments $A = G_i$, and for chiral environments $A = H_i$ (of order $i/2$), where H_i is a normal subgroup of G_i consisting of all the permutations in G_i. The number of double cosets is given by

$$\frac{|G_{36}|}{|A|\cdot|L_j|}\sum_{r=1}^{9}\frac{|A\cap C_r|\cdot|L_j\cap C_r|}{|C_r|}$$

where C_r is one of the nine conjugacy classes in G_{36}.[17]

(67) The term "maximally labeled"[19a] signifies that the identity is the only symmetry element in the MSG of the unlabeled structure capable of generating an isometric structure from a maximally labeled one. That is, the MSG of a maximally labeled structure consists only of the identity. The isomer count assumes its maximum value for such a structure (cf. L_1 in Table X), though the converse does not always follow (e.g., cf. L_{2b} and L_1 under G_{12}, Table X). The substitution pattern listed for L_1 in Table X (AAAABABC) is thus a valid representation of a maximally labeled structure, even though there is a redundancy of ligands (i.e., of A and B).

Table X. Substitution Patterns for Derivatives of 1-3 and Corresponding Isomer Counts under the Operation of Selected Rearrangement Modes

permutation/ permutation-inversion group	space group	representative substitution pattern[a]								isomer count[b] for subgroups G_i[c]				
		a	b	1	2	3	4	5	6	G_{36}	G_{12}	G_{4a}	G_{4b}	G_2
$L_{36} = (C_3)^2 \wr V$	$c2mm\ 3^2$	A	A	A	A	A	A	A	A	1/0	1/0	1/0	1/0	0/1
$L_{18a} = (C_3)^2 \wr C_{2a}$	$c211\ 3^2$	A	A	A	A	A	B	B	B	1/0	1/0	1/0	1/0	0/1
$L_{18b} = (C_3)^2 \wr C_{2b}$	$c1m1\ 3^2$	A	A	F	F	F	F	F	F	0/1	0/1	0/1	0/1	0/2
$L_{18c} = (C_3)^2 \wr C_{2c}$	$c11m\ 3^2$	A	B	A	A	A	A	A	A	1/0	1/0	1/0	1/0	0/1
$L_9 = (C_3)^2 \wr C_1$	$c111\ 3^2$	A	B	A	A	A	B	B	B	0/1	0/1	0/1	0/1	0/2
$L_6 = (C_3 \times C_1) \wr C_{2a}$	$c211\ 31$	A	A	A	A	A	A	A	B	1/0	1/0	1/1	1/1	0/3
$L_3 = (C_3 \times C_1) \wr C_1$	$c111\ 31$	A	A	A	A	A	A	B	C	0/1	0/1	0/3	0/3	0/6
$L_4 = (C_1)^2 \wr V$	$c2mm\ 1^2$	A	A	A	A	B	A	A	B	1/0	1/1	2/2	2/2	0/6
$L_{2a} = (C_1)^2 \wr C_{2a}$	$c211\ 1^2$	A	A	A	A	B	A	B	B	1/0	1/1	1/4	1/4	0/9
$L_{2b} = (C_1)^2 \wr C_{2b}$	$c1m1\ 1^2$	A	A	A	B	C	A	C	B	0/1	0/3	0/6	0/6	0/12
$L_{2c} = (C_1)^2 \wr C_{2c}$	$c11m\ 1^2$	A	A	A	B	C	A	B	C	1/0	1/1	3/3	3/3	0/9
$L_1 = (C_1)^2 \wr C_1$	$c111\ 1^2$	A	A	A	A	B	A	B	C	0/1	0/3	0/9	0/9	0/18

[a] A, B, and C are achiral ligands; F is a chiral ligand. Numbering of ligand sites refers to skeleton A (text). [b] For each entry (u/v), u = number of meso (achiral) isomers and v = number of racemic (DL) pairs.[63] [c] $G_{12} = \{1, 6, 7, 10, 11, 12, 19, 23, 27, 28, 34, 35\}$, $G_{4a} = \{1, 10, 22, 29\}$, $G_{4b} = \{1, 10, 27, 28\}$, $G_2 = \{1, 10\}$. The elements of the sets correspond to group element numbers in Table I.

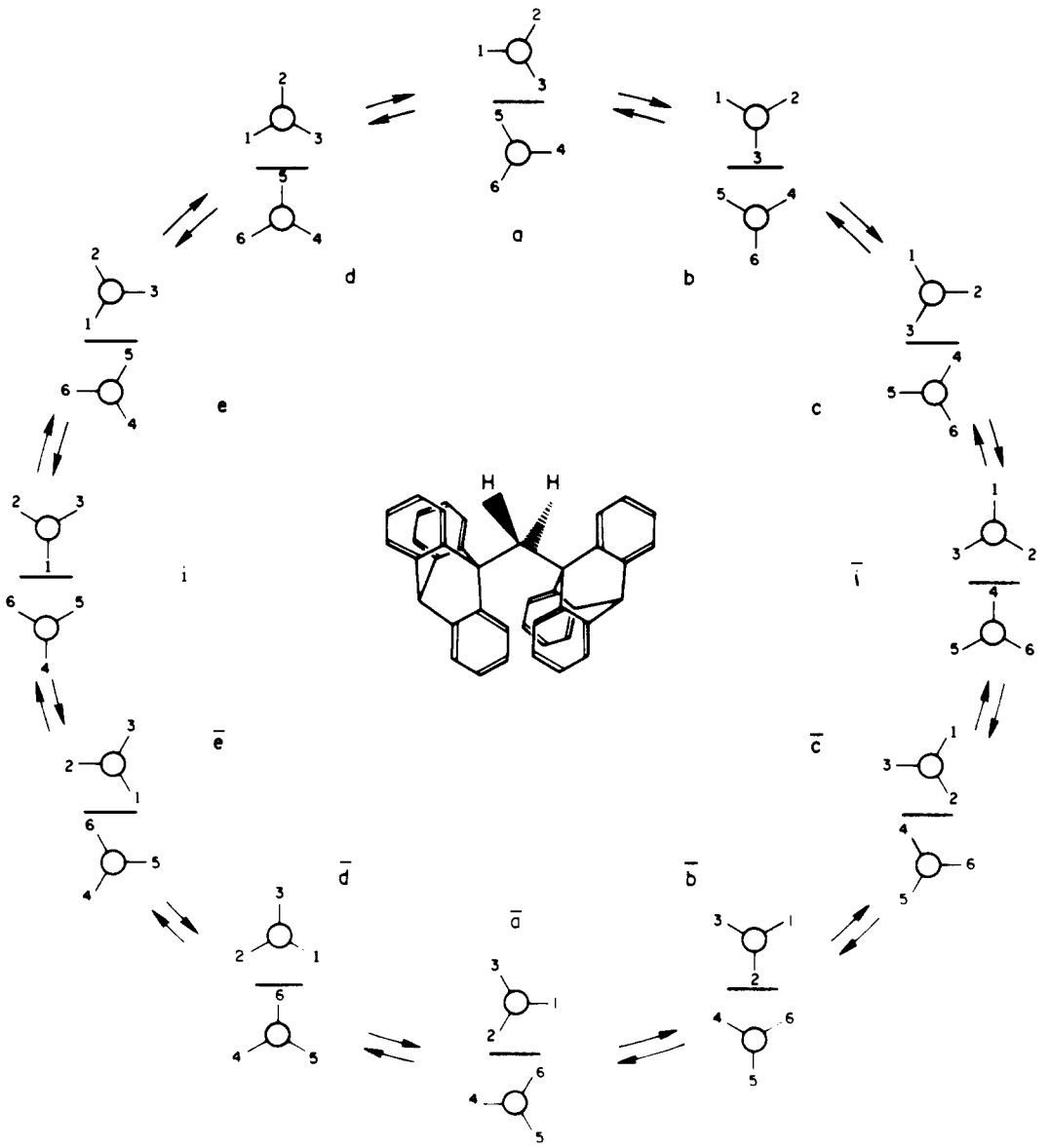

Figure 6. Conformational gearing circuit for bis(9-triptycyl)methane (**3**), with projections following the convention for B. Letters correspond to the points on the PE hypersurface shown in Figure 4. A representative structural formula for **3** (approximate C_s symmetry) is shown in the center.

For derivatives of **3**, appropriate G_i's for Tp group rotation are G_{36} ($Z = 1$), G_{12} ($Z = 3$), and G_2 ($Z = 18$), in order of decreasing times scales of observation. Under conditions of rapid gearing and gear slippage (see above), G_{36} applies, and one ressidual DL

pair is expected for a maximally labeled derivative. It may be safely anticipated that such conditions will be attainable only at elevated temperatures, given the magnitude (30.1 kcal mol^{-1}) of the calculated gear-slippage barrier. By the same token, under ordinary laboratory conditions only gearing remains rapid (G_{12}), and three residual DL pairs are anticipated for a maximally labeled structure.[69] Finally, in the event that both processes are frozen out, there should be 18 DL pairs for a maximally labeled structure; given the magnitude of the calculated barrier (0.19 kcal mol^{-1}), however, this is unlikely to be observed in the absence of a major perturbation of the PE hypersurface.[61]

Minimal Labeling. The minimum degree of labeling necessary to distinguish between different rearrangement modes can be derived from Table X by considering that a distinction between two modes is possible if a given labeling pattern shows different numbers of isomers, depending on which rearrangement mode is operational. Thus, for **3**, G_{12} (gearing) and G_{36} (gearing and gear slippage) both lead to one meso species if we label only one Tp group (e.g., L_6). When both Tp groups are substituted equivalently (L_4), the mode G_{36} leads to one meso species but G_{12} leads to a meso isomer *plus* a DL pair. In principle, these may be distinguished spectroscopically. Though similar results are obtained for more complicated substitution patterns, the pattern L_4 is the simplest one that can still distinguish between G_{12} (gearing) and G_{36} (gearing and gear slippage).

(68) Experimental support has been adduced from a scatter plot of torsional coordinates (ϕ, ϕ') for the two CC_3 rotors in structural fragments of the type C_3C–C–CC_3: Nachbar, R. B., Jr.; Johnson, C. A.; Mislow, K. *J. Org. Chem.* **1982**, *47*, 4829.

(69) For a $C_s(2/1)$ ground state,[53] the double coset representing gearing generates the same group G_{12} and therefore the same isomer table (G_{12b} in ref 4).

Summary

Group theory has been used to enumerate all isometric structures of molecules **1**, **2**,[16] and **3**, as well as all rearrangement modes. Each such mode interconverts some or all of the isometric structures; i.e., it partitions them into sets (or isomers) such that interconversion occurs between isometric structures within but not among sets. In order to distinguish different sets, we find that the molecule under investigation must be labeled in such a manner that different sets (or isomers) have different physical properties. Some labeling patterns lead to different numbers of isomers, depending on the effective rearrangement or interconversion mode, and can therefore be used to distinguish among different modes. With the help of EFF calculations, some of the rearrangement modes have been associated with detailed mechanisms, i.e., with detailed changes in geometry and energy occurring during the interconversion. Specifically, our analyses and calculations lead to the prediction that of the three compounds studied, only **3** is capable of existing in suitably derivatized isomeric forms at ambient temperature, i.e., under ordinary laboratory conditions. A test of this prediction is described in the following paper.[70]

Acknowledgment. We thank the National Science Foundation (CHE-8009670) for support of this work. H.B.B. thanks the chemistry faculty at Princeton University for their hospitality during his stay in the spring term of 1981.

Registry No. 1, 74-98-6; **2**, 1070-87-7; **3**, 73611-46-8.

(70) Guenzi, A.; Johnson, C. A.; Cozzi, F.; Mislow, K. *J. Am. Chem. Soc.*, following paper in this issue.

Dynamic Gearing and Residual Stereoisomerism in Labeled Bis(9-triptycyl)methane and Related Molecules. Synthesis and Stereochemistry of Bis(2,3-dimethyl-9-triptycyl)methane, Bis(2,3-dimethyl-9-triptycyl)carbinol, and Bis(1,4-dimethyl-9-triptycyl)methane[1]

Alberto Guenzi, Constance A. Johnson, Franco Cozzi, and Kurt Mislow*

Contribution from the Department of Chemistry, Princeton University, Princeton, New Jersey 08544. *Received May 10, 1982*

Abstract: The substitution patterns of bis(9-triptycyl)methane (**1**) and -carbinol (**2**), two molecular bevel gear systems, have been classified according to the number of residual stereoisomers remaining under the full operation of the gearing mode and in the presence or absence of gear-slippage constraints. Substitution patterns have been identified in which enantiomeric conformations are interconverted by gearing through exclusively chiral pathways. Bis(2,3-dimethyl-9-triptycyl)methane (**3**) and -carbinol (**4**) have each been separated into residual meso and DL isomers, and the isomers have been unambiguously identified by NMR spectroscopy. *meso*-**3** (**3a**) and DL-**3** (**3b**) are interconverted at elevated temperatures by a gear-slippage mechanism; the diastereomerization barrier (ΔG^*) is 34 kcal mol^{-1} at 145–165 °C. The racemization barrier of **3b**, which also involves gear slippage, is found to be >22 kcal mol^{-1}. These findings are in accord with an empirical force field (EFF) prediction of 30 kcal mol^{-1} for the gear-slippage barrier in **1**. The methyl groups in the 1- and 1′-positions of *meso*-bis(1,4-dimethyl-9-triptycyl)methane (**5a**) restrict cogwheeling of the 9-triptycyl groups, and a gearing barrier is therefore measurable by dynamic NMR. The measured ΔG^* of 14 kcal mol^{-1} is comparable to a barrier of 17 kcal mol^{-1} calculated (EFF) for the conformational interconversion by the gearing mechanism. The gear-slippage barrier, as measured by conversion of **5a** to the DL isomer (**5b**), is 39 kcal mol^{-1} at 215 °C. The present work describes the first measurement of stereoisomerization barriers resulting from restricted gearing and gear slippage.

Empirical force field (EFF) calculations reported in the preceding paper[2] have shown that the 9-triptycyl (Tp) moieties in bis(9-triptycyl)methane[3] (**1**) undergo virtually unhindered correlated disrotation (dynamic gearing). The molecule has a C_2

0002-7863/83/1505-1438$01.50/0